Nanoscale

Maximization of thermal conductance at interfaces via exponentially mass-graded interlayers

Journal:	*Nanoscale*
Manuscript ID	NR-ART-11-2018-009188.R2
Article Type:	Paper
Date Submitted by the Author:	22-Feb-2019
Complete List of Authors:	Rastgarkafshgarkolaei, Rouzbeh; University of Virginia Zhang, Jingjie; University of Virginia, Polanco, Carlos; Oak Ridge National Laboratory Le, Nam; US Naval Research Laboratory Ghosh, Avik; University of Virginia, Dept. of Electrical and Computer Engineering Norris, Pamela; University of Virginia

Journal Name

ARTICLE TYPE

Cite this: DOI: 10.1039/xxxxxxxxxx

Maximization of thermal conductance at interfaces via exponentially mass-graded interlayers†

Rouzbeh Rastgarkafshgarkolaei,[*,a,⊥] Jingjie Zhang,[§,b,⊥] Carlos A. Polanco,[d] Nam Q. Le,[e] Avik W. Ghosh,[b,c] Pamela M. Norris[a,‡]

Received Date
Accepted Date

DOI: 10.1039/xxxxxxxxxx

www.rsc.org/journalname

We propose a strategy to potentially best enhance interfacial thermal transport through solid–solid interfaces by adding nano-engineered, exponentially mass-graded intermediate layers. This exponential design rule results in a greater enhancement than a linearly mass-graded interface. By combining calculations using non-equilibrium Green's functions (NEGF) and non-equilibrium molecular dynamics (NEMD), we investigated the role of impedance matching and anharmonicity in the enhancement in addition to geometric parameters such as the number of layers and the junction thickness. Our analysis shows that the effect on thermal conductance is dominated by the phonon thermalization through anharmonic effects, while elastic phonon transmission and impedance matching play a secondary role. In the harmonic limit, increasing the number of layers results in greater elastic phonon transmission at each individual boundary, countered by the decrease of available conducting channels. Consequently, conductance initially increases with number of layers due to improved bridging, but quickly saturates. The presence of slight anharmonic effects (at very low temperature, **T** = 2 K) turns the saturation into a monotonically increasing trend. Anharmonic effects can further facilitate interfacial thermal transport through the thermalization of phonons at moderate temperatures. At high temperature, however, the role of anharmonicity as a facilitator of interfacial thermal transport reverses. Strong anharmonicity introduces significant intrinsic resistance, overruling the enhancement in thermal conduction at the boundaries. It follows that at a particular temperature, there exists a corresponding junction thickness at which thermal conductance is maximized.

New challenges for thermal management of semiconductor devices have arisen due to the miniaturization of present day electronics to the nanoscale[1]. For such devices, thermal resistance at material interfaces limits heat dissipation, increases their operating temperature, and ultimately impacts their performance and reliability[2]. The heat dissipation problem of semiconductor devices can be mitigated using high thermal conductivity materials, like diamond, as heat spreaders. However, this approach is limited by the thermal resistance at material interfaces arising inside and in between devices, as well as their connections to external bias and contact pads[3–6]. Thus, thermal resistance at interfaces is a critical bottleneck for thermal management of semiconductor devices and concerted efforts are now focused on reducing this resistance[7–9].

Thermal conduction at an interface can be enhanced by varying interfacial properties such as roughness[10], atomic composition and bonding[11–16]. By strengthening the bonds at a junction, for example, phonon transmission across the interface can be made to increase, along with the corresponding thermal conductance[17–22]. The interfacial geometry can also influence thermal transport across material interfaces by providing larger effective interfacial contact area[23]. Even interatomic mixing at the interface can result in an increase in conductance due to the introduction of new transport channels across the interface[24–26]. Moreover, it has been shown that anharmonic interactions significantly facilitate heat transfer across solid-solid interfaces[27].

To enhance interfacial conductance, one proposed approach

[a] *Department of Mechanical and Aerospace Engineering, University of Virginia, Charlottesville, Virginia 22904, USA.*
[b] *Department of Electrical and Computer Engineering, University of Virginia, Charlottesville, Virginia 22904, USA.*
[c] *Department of Physics, University of Virginia, Charlottesville, Virginia 22904, USA.*
[d] *Materials Science and Technology Division, Oak Ridge National Laboratory, Oak Ridge, Tennessee 37831, USA.*
[e] *National Research Council Research Associateship Programs, Code 6189, U.S. Naval Research Laboratory, Washington, District of Columbia 20375, USA.*
∗ Email: rr3ay@virginia.edu
§ Email: jz9wp@virginia.edu
‡ Email: Pamela@virginia.edu
⊥ These authors contributed equally to this work.
† Electronic Supplementary Information (ESI) available: [details of any supplementary information available should be included here]. See DOI: 10.1039/b000000x/

is the insertion of a thin (∼nm) intermediate layer at the interface[21,24,28–32], similar to applications of anti-reflective (AR) coatings in photonics[33]. In the harmonic limit, the layer increases the elastic transmission of phonon modes as well as the overlap of phonon density of states (PDOS) of the materials at the newly formed interfaces and acts as a "phonon bridge"[24]. Previously, we showed that anharmonic processes play a key role in the enhancement of thermal conduction in these systems in comparison with the purely harmonic limit[31]. At each material junction, those processes help phonons thermalize to frequencies with higher transmission rates and thus they can increase the thermal conductance[34]. Moreover, anharmonic processes decouple the two material interfaces abutting the thin layer and thus the system resistance can be represented as the sum of the boundary resistances plus a junction resistance[31]. This generates an optimum condition: since each interfacial resistance depends on the ratio of the acoustic impedances on each side, the maximum thermal conductance happens when the atomic mass (i.e., impedance for constant bond stiffness) of the layer is the geometric mean of the contact masses[31], which we refer to as the "geometric mean rule" throughout the rest of this article.

In this work, we refer to the *additive* transport regime, in which interfaces become decoupled and we observe that thermal resistances are additive due to incoherence[35]. Commonly, it is thought that the overall resistance at a bridged interface equals the sum of interfacial and intrinsic resistances only when transport is diffusive, i.e. when the mean free path (MFP) of phonons becomes smaller than the layer thickness. However, we have shown previously[31] that at bridged interfaces, the total resistance is still well approximated by the sum of resistances despite layer thicknesses smaller (∼nm) than the bulk phonon MFP. Based on our definition, the diffusive limit is the extreme limit for the additive regime in terms of increasing phonon scattering.

Building on our previous work with a monolithic bridging interface[31,34], in this paper we explore the enhancement of thermal conductance of a *mass-graded* interface or an interface with several intermediate thin layers (Fig. 1) analogous to the design of refractive index-graded AR coatings[36,37]. The atomic mass of each layer (m_n) is chosen based on the geometric mean rule relative to its neighboring layers, which corresponds to an exponential change of the atomic masses from the left contact mass (m_l) to the right contact mass (m_r) described by:

$$m_n = m_l e^{\zeta n}, \tag{1}$$

with $\zeta = \ln(m_r/m_l)/(N_l+1)$. We show that this choice of masses can lead to a conductance enhancement ($\sim 53\%$ with fixed layer thickness [$t = 6$ u.c. and $L = 24$ u.c. in Fig. 7] or $\sim 56\%$ with fixed junction thickness [$t = 1$ u.c. and $L = 6$ u.c. in Fig. 7]. Those enhancements are relative to the conductance of the abrupt interface 102.40±1.70 MW m^{-2} K^{-1}) about two times larger than the best enhancement obtained with a single bridging layer studied by Polanco *et al.*[31] ($\sim 23\%$). Moreover, we demonstrate larger enhancement compared to a previously proposed linearly mass-graded interface[38] (Sec. 5). Our results examine the influence of the number of layers N_l and the thickness of the layers t (Fig. 1) on the thermal conduction across mass-graded interfaces.

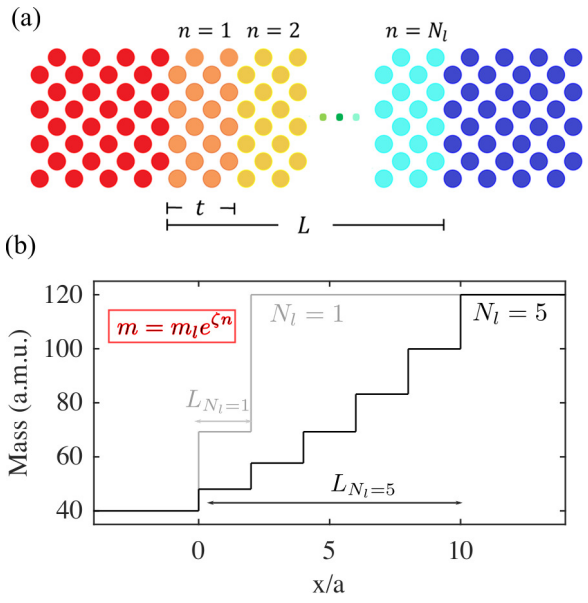

Fig. 1 (a) Schematic of a mass-graded interface with N_l layers. In this case, each layer has a thickness of 2 unit cells ($t = 2$ u.c.) and the thickness of the junction is $L = t \times N_l$ u.c. (b) The spatial variation of masses for N_l=1 and N_l=5 (t=2 u.c.). m_l and m_r are 40 a.m.u. and 120 a.m.u. respectively and a is the lattice constant for 1 u.c.

Besides studying the influence of geometric parameters, we also explore the effect of varying the strength of anharmonicity on the conductance. Non-equilibrium Green's function (NEGF) and non-equilibrium molecular dynamics (NEMD) simulations are used to compare interfacial thermal transport without anharmonic processes at **T** = 0 K (Sec. 2), with weak anharmonicity at low temperature of 2 K (Sec. 3), and with strong anharmonicity at medium temperature of 30 K (Sec. 4). We find that the strength of anharmonicity determines how different geometric properties of the mass-graded junction influence the conductance. In the limit of weak anharmonicity, increasing the junction thickness facilitates thermal transport by phonon thermalization. In the limit of strong anharmonicity, however, increasing the layer thickness over the optimum thickness increases phonon back scattering and suppresses thermal transport. Our results suggest that in our model Lennard-Jones system, anharmonic effects contribute mostly to the enhancement in the conductance associated with insertion of a mass-graded junction while contributions from elastic phonon transmission come secondary.

1 Methodology

The focus of our study is mass-graded interfaces (Fig. 1), with the atomic mass of each intermediate layer varying exponentially from the left to the right contact according to Eq. 1. All atomic interactions in the system are dictated by the same Lennard-Jones (LJ) potential (see section A in Supporting information). The system has a single atom per primitive unit cell and a face-centered cubic crystal structure. Thermal conductance (G) across the mass-graded interface is defined as the ratio between the heat flux (q) crossing the interface and the temperature drop across the entire

junction ($\Delta\mathbf{T}$):

$$G = \frac{q}{\Delta\mathbf{T}}. \quad (2)$$

To calculate G using Eq. 2 within NEMD, we prescribe a constant temperature difference over the simulation box. Upon reaching a steady state temperature profile, we fit the temperature data at the contacts with linear profiles, which are extrapolated to the external edges of the first and last intermediate layers to define $\Delta\mathbf{T}$. Heat flux q is calculated by monitoring the cumulative energy added/subtracted to the hot/cold Langevin baths. We calculate thermal conductance at $\mathbf{T} = 2$ K and $\mathbf{T} = 30$ K, which are 0.7% and 10% of the melting temperature, to explore the phonon transport in the limit of weak and strong phonon-phonon interactions.

The conductance in the limit of zero phonon-phonon interactions is calculated using harmonic NEGF[39,40]. To compare these simulations with the NEMD results, we take the classical limit of the Bose-Einstein distribution ($\hbar\omega_{cut} \ll k_B\mathbf{T}$) and compute the conductance as[31]:

$$G_{hl} = \frac{k_B}{2\pi A}\int_0^\infty d\omega MT, \quad (3)$$

where $\hbar\omega_{cut}$ is the maximum phonon energy, k_B is the Boltzmann constant, A is the cross-sectional area, M is the number of modes contributing to transport, and T is the average transmission per mode. MT is calculated using the NEGF formalism as $MT = \mathrm{Tr}[\Gamma_l G^r \Gamma_r G^{r\dagger}]$, where G^r is the retarded Green's function describing the vibrational dynamics of the interface and $\Gamma_{l,r}$ are the broadening matrices describing how the modes in the contacts interact with the intermediate layers[35,41,42]. Equation 3 shows that G_{hl} is a summation of modes times transmission over the entire frequency spectra, meaning that M and T are the two components determining the conductance. Further details of all numerical calculations are provided in Supporting information.

The analysis of our mass-graded interfaces in the harmonic limit is simplified using the system symmetry. Since all the material boundaries are perfectly abrupt, the potential energy is translationally invariant in the transverse direction, parallel to the boundaries. Thus, the force in that direction is zero and only phonons that conserve their transverse momentum or wavevector ($k_\perp$) can contribute to thermal transport. We define the number of combinations of phonons that conserve momentum along the system as the number of conserving channels M_c and count them using[31]

$$M_c(\omega) = \sum_{k_\perp} \min_\alpha M_\alpha(\omega, k_\perp), \quad (4)$$

with α varying over the contacts and intermediate layers. M_α is the number of propagating modes in material α, which can be obtained by calculating MT from NEGF for each bulk material. In that case, the transmission for each mode is unity and thus $MT = M$. Since the conserving modes are the only ones that contribute to transport, we define an average transmission over those modes as $T_c(\omega) = MT(\omega)/M_c(\omega)$. Replacing MT in Eq. 3 by $M_c T_c$ allows us to separate G_{hl} into a phase space of available transport channels, M_c, and its average phonon transmission, T_c.

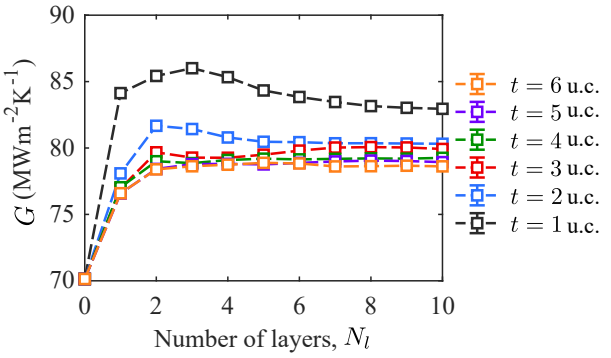

Fig. 2 G_{hl} vs. N_l in the harmonic limit. G_{hl} quickly saturates as N_l increases.

2 Harmonic limit

Figure 2 shows the conductance across mass-graded interfaces in the harmonic limit. As the number of intermediate layers N_l increases, the harmonic conductance initially increases but saturates after $N_l > 5$. This trend is due to the interplay (see Eq. 3) between increasing transmission T_c (Fig. 3(a) and (d)) but decreasing number of transport channels M_c (Fig. 3(a) and (c)). The gain in T_c is due to the decrease in thermal impedance (acoustic impedance in linear dispersion regime) mismatch between adjacent layers[7,43]. This gain happens mostly below 10 Trad/s (Fig. 3(d)) and is responsible for the increase of $MT(\omega)$ over the same frequency range (Fig. 3(b)) since M_c does not change much in that range. Note that the cut-off frequency for the lowest acoustic branch is 10.98 Trad/s, which seems to suggest that decreasing the mass mismatch helps phonon transmission for states with similar polarization (Fig. S1). The monotonic decrease of M_c follows from Eq. 4 as adding more intermediate layers can only decrease the minimum of modes at each $k_\perp$ and ω. The interplay between M_c and T_c yields a modest conductance enhancement in the saturated regions ($N_l > 5$ in Fig. 2), between 11% and 17%.

The saturation of G_{hl} follows from a combined saturation of M_c and T_c. $M_c(\omega, k_\perp)$ is obtained taking the minimum of modes (Eq. 4) over a set of materials with the same force constants and crystal structure, but with masses varying exponentially from one contact to another. Thus the dispersions and $M_\alpha(\omega, k_\perp)$ for those materials change gradually according to the mass. As N_l increases, the interval of this function is sampled more finely by the set of $M_\alpha(\omega, k_\perp)$, and thus M_c saturates to the lower bound. The transmission enhancement also saturates as it approaches its maximum value, unity (Fig. 3(d)).

The conductance of a mass-graded junction does not only depend on the number of layers, it also depends on the thickness of each layer t (Fig. 2). Thin layers yield larger conductance, but this enhancement disappears at about $t = 3$ u.c. We attribute the sharp increase in G_{hl} when the layer thickness is ultra-thin to phonon tunneling. For very thin layers (in our case, 2–3 conventional unit cells), phonons can tunnel even when the middle layers do not have propagating modes at a particular ω and momentum $k_\perp$ but the adjacent materials do. The transport of those extra phonons across the system enhances the overall conductance. This phe-

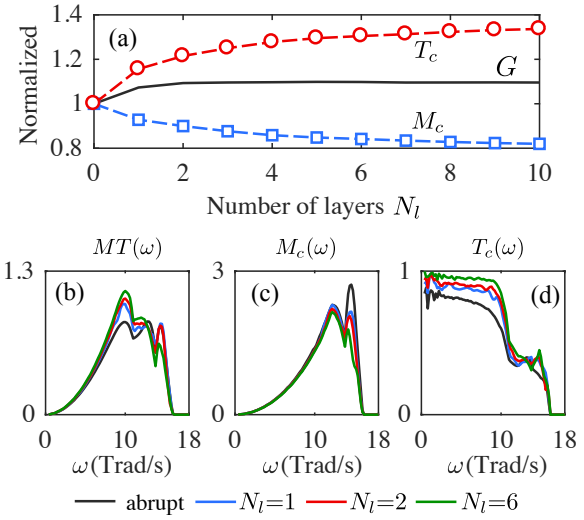

Fig. 3 (a) Normalized values of G_{hl}, M_c, and T_c with respect to the abrupt interface vs. N_l. $M_c = \int_0^\infty M_c(\omega)d\omega$ and $T_c = \int_0^\infty T_c(\omega)d\omega$. T_c increases while M_c decreases with N_l, leading to the saturation of G_{hl}. NEGF results of (b) number of modes times transmission MT(ω), (c) number of available modes $M_c(\omega)$ and (d) average transmission $T_c(\omega) = \frac{MT(\omega)}{M_c(\omega)}$ when N_l is 0 (abrupt), 1, 2 and 6. All simulations are performed for $t = 6$ u.c. Enlarged versions of figures (b)-(d) can be found in the Supplemental Information for a better visualization.

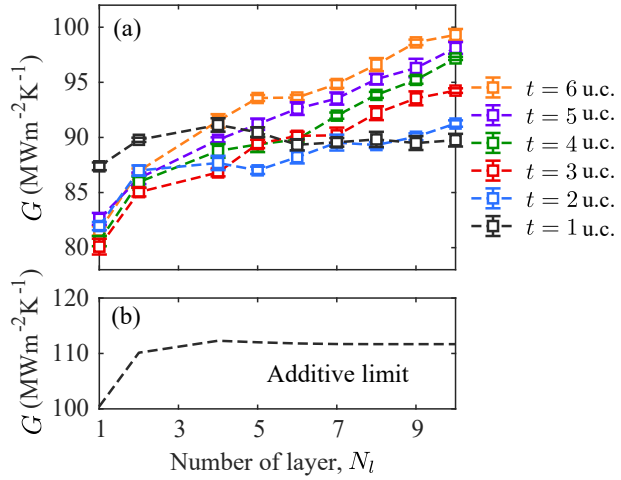

Fig. 4 G vs. N_l in the presence of anharmonicity at **T** = 2 K when the layer thicknesses vary from 1 u.c. to 6 u.c. (a) NEMD results. G increases almost linearly with N_l. Furthermore thicker layers yield larger G_{al}. b) additive limit (Eq. 5). G_{al} increases with N_l and quickly saturates.

nomenon was previously observed by English *et al.*[24] and Liang and Tsai[28] and they related it to the resulting sharp and narrow density of states associated with the thin film which can influence the elastic vs. inelastic thermal transport at the boundaries.

3 Weakly anharmonic limit

Surprisingly, at low temperature when anharmonicity is weak, the trend of G vs. N_l from our NEMD simulations (Fig. 4(a)) differs from that obtained in the harmonic limit by NEGF. We were expecting similar trends because at low temperature (**T** = 2 K, which is about 1% of the melting temperature), atomic displacements in our NEMD simulation are small and thermal transport should be mostly harmonic. Nevertheless, this expectation seems to hold only for systems with $t = 1$ u.c. and $N_l < 10$, where we see a peak followed by a saturation (Fig. 2 and 4(a)). We have verified that the observed trends do not result from size effects on the simulation domains (see section A in Supporting information).

The increasing trend of G vs N_l in our ultra-low temperature NEMD simulations (Fig. 4) is not dictated by additive phonon transport either. In the additive limit, the conductance of the system, G_{al}, can be defined as the inverse of the sum of resistances:

$$1/G_{al} = \sum_{i=1}^{N_l} 1/G_{blk,i} + \sum_{j=1}^{N_l+1} 1/G_{int,j}, \quad (5)$$

where $1/G_{blk,i} = t/\kappa_i$ is the resistance intrinsic to the i^{th} intermediate layer, κ_i is the intrinsic thermal conductivity of material i and $1/G_{int,j}$ is the interfacial resistance for the j^{th} boundary. We neglect $1/G_{blk,i}$ in our analysis since it is significantly less than $1/G_{int,j}$ at **T** = 2 K. For instance for a mass-graded interface with $t = 6$ u.c. and $N_l = 5$, the temperature drop at the interfaces is 93% of the total drop between the contacts (Fig. S2). Figure 4(b) shows the trend of G_{al} vs. N_l with each $G_{int,j}$ calculated on a single, independent boundary using NEGF (Eq. 3) and neglecting $1/G_{blk,i}$. G_{al} initially increases as neighboring layers become more similar and then saturates. The saturation is not seen in NEMD results and thus we conclude that the monotonic increase of conductance at very low temperatures results from neither purely harmonic nor additive transport.

The increasing trend in Fig. 4 hints at the important role played by phonon-phonon interaction in enhancing the conductance of mass-graded interfaces. Conductance seems to increase linearly with N_l and the slope increases with t. Larger N_l and t values result in a thicker total junction length, L, which allows more phonon-phonon scattering in this region. Given the conductance increases as phonon-phonon scattering increases, we hypothesize that scattering promotes thermalization that helps high frequency phonons with lower chance of transmission jump to modes with lower frequencies and higher transmission. This behavior is similar to the linear increase of interfacial thermal conductance with temperature, in which stronger anharmonicity contributes to better thermalization in the neighborhood of the interface[31,34].

The contributions to the enhancement of G from both anharmonicity and elastic phonon transmission are further analyzed in Fig. 5. Conductance increases with L with a similar slope when $t > 1$, suggesting that anharmonicity constitutes the major contribution in the enhancement. This idea is further supported by comparing the enhancement from varying N_l while fixing L (i.e. varying phonon transmission at a fixed strength of anharmonicity) with the results from fixed N_l while varying L (varying the strength of anharmonicity with fixed phonon transmission). Figure 5 suggests that the contribution from the latter is larger than the former. To make this argument quantitative, we turn to the conductance values shown in the inset of Fig. 5. At a fixed $L = 30$ u.c., doubling N_l results in only 3% enhancement in G, whereas at a fixed N_l, increasing L from 30 to 60 u.c. results in more than 7% improvement in conductance. When fixing L, the enhance-

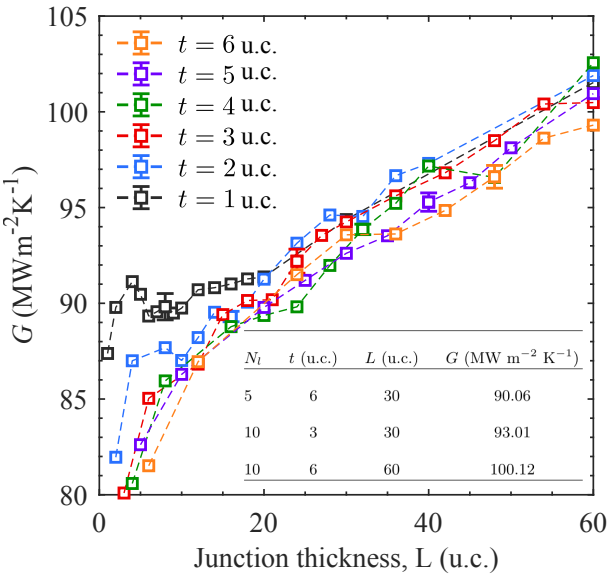

Fig. 5 Interfacial thermal conductance values from NEMD simulations at **T** = 2 K for different junction thicknesses. Each color represents a different sub-layer thickness. Note that total thickness $L = N_l \times t$. Sample error bars are shown at L = 8, 16, 24, 32, 40, and 48 u.c. (inset) conductance values are shown for three cases of varying number of layers, layer's thickness and junction thickness based on an linear fitting in Fig.S4.

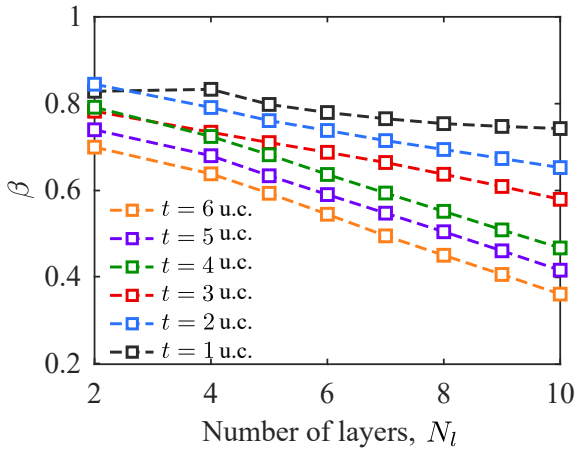

Fig. 6 Contribution to G from harmonic vs. additive phonon transport across various mass graded junctions ($G = \beta G_{hl} + (1-\beta)G_{al}$). $\beta = 1$ represents purely harmonic transport while $\beta = 0$ purely additive transport.

ment would solely be due to increases in phonon transmission at the boundaries; however, this enhancement is very small without the presence of anharmonicity. Bridging layers not only introduce better matching at each boundary, but also provide phonons with opportunity for thermalization, providing thereby a larger contribution to the overall enhancement.

The values of G in the weak anharmonic limit (Fig. 4(a) and 5) are bounded by those in the harmonic limit (lower bound) (Fig. 2) and those in the additive limit (upper bound) (Fig. 4(b)). Also, as N_l or L increases, G seems to transition from the harmonic to the additive limit. To quantify the ratio of harmonic vs. additive phonon transport across the junction, we define a quantity β such that $G = \beta G_{hl} + (1-\beta)G_{al}$, where the harmonic conductance G_{hl} is obtained from NEGF (Eq. 3) calculations across multiple layers in the same way Fig. 2 was obtained, while the additive limit conductance G_{al} is obtained from Eq. 5 by adding NEGF calculations at single boundaries exactly like Fig. 4(b) was obtained. Figure 6 shows that as N_l increases, G approaches the additive limit and thus β decreases, meaning less phonons can transport across all the interfaces without being scattered by other phonons. This is consistent with our conjecture that the bridging layers facilitate more phonons participating in the thermalization process.

4 Strongly anharmonic limit

Conductance values from NEMD simulations at high temperature (**T** = 30 K), when anharmonicity is strong, are plotted in Fig. 7. The trend of G vs. L results from the interplay between the interfacial $G_{int,j}$ and intrinsic $G_{blk,i}$ conductances in Eq. 5. Table 1 explains the opposite influences of these two conductance terms quantitatively. For constant layer thickness t, when N_l increases from 2 to 7, the overall conductance G increases because of higher phonon transmission at individual boundaries which increases the interfacial conductances $G_{int,j}$. Moreover, in this regime, extra phonon-phonon scattering provided by larger L enhances the conductance through phonon thermalization, also resulting in higher $G_{int,j}$ values. G then reaches a maximum at junction thicknesses around 20-30 u.c. When N_l increases from 7 to 10, G decreases with the junction thickness because the gain of conductance at the boundaries $G_{int,j}$ is overshadowed by the decrease in the layers' intrinsic conductance $G_{blk,i}$. Consequently, the maximum G is dictated by the interplay between the intrinsic phonon-phonon resistance of the mass-graded junction ($1/G_{blk,i}$) and the interfacial resistance at each individual boundary ($1/G_{int,j}$).

This interplay is mainly driven by the strength of anharmonic processes in the system. To elaborate, we observed in Fig. 5 that at low temperature when anharmonicity is weak, extra anharmonicity provided by thicker junctions can enhance the transport. On the other hand, in Fig. 7 when anharmonicity is strong, extra anharmonic scattering will be detrimental to the overall transport. In both of these scenarios, the potential enhancement from higher elastic transmission of phonons at the boundaries is subtle. These observations show that the influence of a bridging layer on thermal conductance is dominated by the phonon thermalization through anharmonic effects.

Figure 8 shows the effects of anharmonicity on the thermal conductance of mass graded interfaces, both as a facilitator in the weak anharmonicity limit and a suppressor in the strong anharmonicity limit. We calculated G keeping the number of layers constant at either $N_l = 8$ or 16, while varying the thickness of each layer t (see Fig. 8). At low temperature, i.e. weak anharmonicity, $G_{blk,i}$ is negligible and thermal conductance increases with junction thickness. This trend flips at high temperatures, shown in Fig. 8, where anharmonicity is strong and $G_{blk,i}$ plays a profound role in hindering thermal transport and consequently, G decreases with junction thickness.

Using the results from this computational work, our goal is to

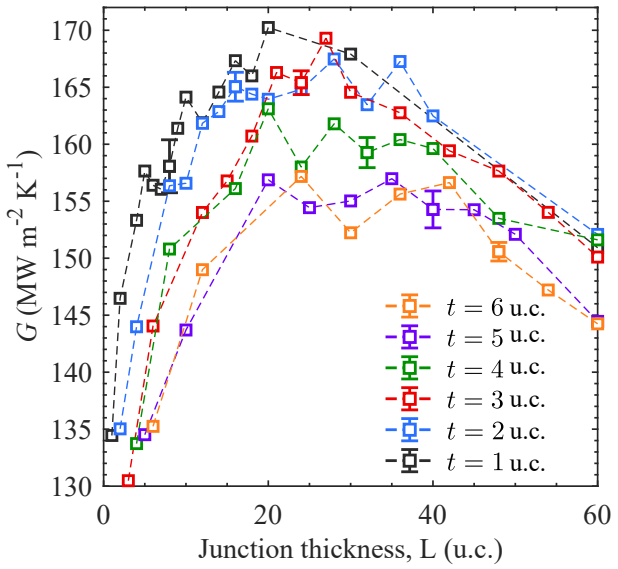

Fig. 7 Interfacial thermal conductance from NEMD simulations at **T** = 30 K for different thicknesses of the junction. Each color represents a different sub-layer thickness. Sample error bars are shown at L = 8, 16, 24, 32, 40, and 48 u.c. The conductance of the abrupt interface is 102.40±1.70 MW m^{-2} K^{-1}.

Table 1 Contribution from interfacial thermal conductance $G_{int,j}$ at individual boundaries and intrinsic conductance $G_{blk,i}$ values to the overall thermal conductance G at **T** = 30 K from NEMD for three cases with equal layer thickness t and different number of layers N_l

t (u.c.)	N_l	$\frac{1}{\sum_i 1/G_{blk,i}}$	$\frac{1}{\sum_j 1/G_{int,j}}$	G (MW m^{-2} K^{-1})
6	2	626.5	195.4	148.9 ± 2.0
6	7	299.9	325.6	156.1 ± 1.2
6	10	240.1	364.8	144.8 ± 0.8

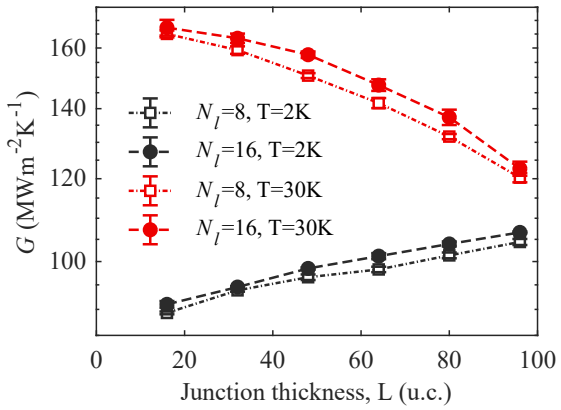

Fig. 8 G vs. total thickness of the graded interface, L, for fixed number of layers (N_l = 8 vs. 16) at low (**T** = 2 K) and high (**T** = 30 K) temperatures.

guide experiments to design engineered interfaces with enhanced thermal conductance including bridging interfaces that can be integrated into devices to achieve superior thermal and electronic performance. It has previously been shown by Wu et al.[44] that a symmetric graded layer of GaAs/In$_x$Ga$_{1-x}$As/GaAs can enhance the electron mobility. Moreover, experimental fabrication of compositionally graded junctions has been enabled by a metal organic chemical vapor deposition (MOCVD) process and thus necessitates an investigation on the effect of the parameters, which can be adjusted during the fabrication, that can alter the thermal transport[45]. A similar fabrication technique may also be used to create an exponentially mass-graded system. For instance, if an Al$_x$Ga$_{1-x}$N layer is added to an AlN/GaN interface, x can be chosen such that the average mass of Al$_x$Ga$_{1-x}$ follow the exponential rule (Eq. 1). Change in material composition across the junction is an important factor that can influence the thermal transport at mass-graded interfaces. In the next section, we compare the level of enhancement in G using two different grading schemes: exponential vs. linear.

5 Exponential vs. Linear

A 6-fold increase of thermal conductance was previously reported[38] for linear mass-graded interfaces. In this section, we aim to compare the percentage of enhancement in two systems: grading the mass along the intermediate layer either linearly or exponentially. We hypothesize that choosing the masses of a mass-graded junction in an exponential fashion (following Eq. 1) minimizes the resistance due to all material boundaries in the system. Therefore, the resistance of an exponentially mass-graded junction is less than that of most other mass-graded choices, including a linearly mass-graded junction. This hypothesis is motivated by our previous works[30,31], which prove it for particular cases. An informal proof of this hypothesis is presented in the Supporting Information highlighting how the exponential variation of masses results directly from the geometric mean rule, which yields close to maximum conductance at an interface with a single intermediate layer. Thus, it is expected that exponentially graded interfaces result in larger enhancement in G.

To test the aforementioned hypothesis, we setup the baseline system with mass mismatch of 10 between the two contacts, i.e. $\frac{m_r}{m_l} = 10$, to replicate the work presented by Zhou *et al.*[38]. We set the junction thickness to be $L = 12$ u.c. and the temperature **T** = 30 K for all the systems, so that the two systems are exactly the same except for the mass of each layer. Our results indicate an extra enhancement in G upon utilizing the exponential mass-graded interface compared to its linear counterpart (Fig. 9). A maximum enhancement of 308% is attained for the exponential mass-graded interface, compared to the linear grading which gives 289% ($N_l = 6$ in Fig. 9). Our results are in line with our previous findings and hypothesis[31], that the enhancement due to a bridging layer can be maximized when the mass of the intermediate layer is close to the geometric mean of the contact masses.

The difference between the conductance values for these two types of interfaces slowly decreases as the number of layers increases. More layers result in smaller mass mismatch at each boundary. Previously[31], we showed that as mass mismatch ($\frac{m_r}{m_l}$)

at the interfaces decreases, a wider range of masses around the geometric mean produce a conductance close to the maximum. Thus, the influence of the geometric mean rule reduces for larger numbers of layers and the exponential and linear mass-graded interfaces exhibit a similar enhancement in thermal conduction.

The percentage of enhancement at these mass-graded interfaces strongly depends on the amount of mass mismatch in the systems. Our results indicate that enhancement in G varies from 68% to 308% as the mass ratio varies from 3 to 10. It is necessary to develop a framework where the reported percentage of enhancement is independent of the vibrational mismatch. This may be done by taking advantage of the dependency of G from the mass ratio at the boundary and maximum phonon frequency present in the system, as shown in our previous work[31].

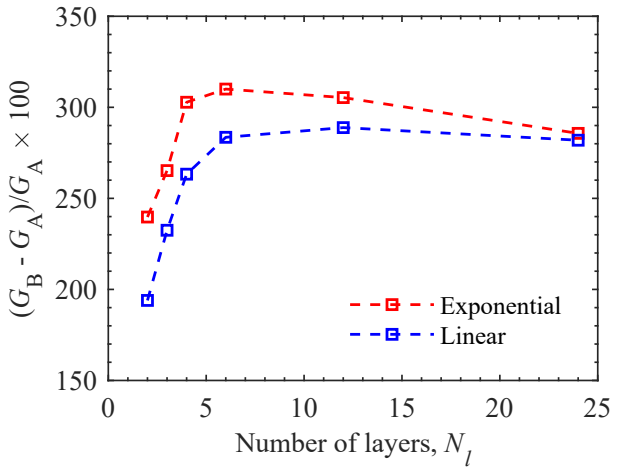

Fig. 9 Comparing enhancement in thermal conductance values (G_B and G_A stand for the conductance of the bridged and abrupt interfaces, respectively) between linearly and exponentially mass-graded interfaces, varying the number of layers at the interface, and keeping the total thickness constant. Junction thickness L for all the cases is 12 u.c. System temperature is set to be **T** = 30 K. ($m_l = 40$ amu , $m_r = 400$ amu)

6 Conclusions

We have demonstrated that the introduction of an exponentially mass-graded junction can enhance thermal conductance beyond its linear graded counterpart. The enhancement of conductance at such interfaces depends on the number of layers, thickness of the junction and the temperature. In the harmonic limit, increasing the number of layers results in better acoustic impedance matching at the boundaries and higher phonon transmission at those individual interfaces and thus facilitates thermal transport. On the other hand, adding more layers in the junction decreases the number of transport channels, consequently hindering the transport. These opposing actions thus result in increasing the overall conductance initially, and then turns into an asymptotic saturation of thermal conductance when the number of layers is large.

We also found that the potential enhancement using a mass-graded junction strongly depends on anharmonicity, which is both influenced by the thickness of the junction and the temperature. Anharmonic processes, however, can have opposing effects on the conductance. At low temperature, when anharmonicity is weak, extra anharmonicity provided by the thicker junctions facilitates transport by thermalizing phonons with higher frequencies to the modes with lower frequencies and higher chance of transmission at the boundaries. In the limit of strong anharmonicity, however, the intrinsic resistance of the junction overshadows the gain in conductance at the boundaries, and consequently extra anharmonicity hinders the transport in this regime. Influence of mass-grading on thermal conductance is dominated by the phonon thermalization through anharmonic effects, while elastic transmission of phonon modes across boundaries plays a secondary role. Lastly, we find that the percentage of enhancement strongly depends on the mass mismatch at the interface, varying from 308% to 68% as the ratio varies from 10 to 3.

Conflicts of interest

There are no conflicts to declare.

Acknowledgements

R.R and P.M.N. acknowledge the financial support of the Air Force Office of Scientific Research (Grant No. FA9550-14-1-0395). J.Z. and A.W.G acknowledge the support from "Graduate opportunity (GO!)" program associated with Center for Nanophase Materials Sciences (CNMS) at Oak Ridge National Laboratory (ORNL). N.Q.L. acknowledges support from the U.S. Naval Laboratory (NRL) through the National Research Council Research Associateship Programs. C.A.P. acknowledges support from the Laboratory Directed Research and Development Program of Oak Ridge National Laboratory, managed by UT-Battelle, LLC, for the U.S. Department of Energy. Computational work was performed using resources of the Advanced Research Computing Services at the University of Virginia and the "Campus Compute Co-operative (CCC)"[46]. The authors are grateful for useful discussions with Prof. Keivan Esfarjani, and LeighAnn Larkin.

References

1 E. Pop, *Nano Res.*, 2010, **3**, 147.
2 G. Riedel, J. Pomeroy, K. Hilton, J. Maclean, D. Wallis, M. Uren, T. Martin, U. Forsberg, A. Lundskog, A. Kakanakova-Georgieva, G. Pozina, E. Janzen, R. Lossy, R. Pazirandeh, F. Brunner, J. Wurfl and M. Kuball, *IEEE Electron Dev. Lett.*, 2009, **30**, 103.
3 J. W. Pomeroy, M. Bernardoni, D. C. Dumka, D. M. Fanning and M. Kuball, *Appl. Phys. Lett.*, 2014, **104**, 083513.
4 H. Sun, J. W. Pomeroy, R. B. Simon, D. Francis, F. Faili, D. J. Twitchen and M. Kuball, *IEEE Electron Dev. Lett.*, 2016, **37**, 621.
5 Y. Zhou, R. Ramaneti, J. Anaya, S. Korneychuk, J. Derluyn, H. Sun, J. Pomeroy, J. Verbeeck, K. Haenen and M. Kuball, *Appl. Phys. Lett.*, 2017, **111**, 041901.
6 J. Cho, D. Francis, D. H. Altman, M. Asheghi and K. E. Goodson, *J. Appl. Phys.*, 2017, **121**, 055105.

7 D. G. Cahill, W. K. Ford, K. E. Goodson, G. D. Mahan, A. Majumdar, H. J. Maris, R. Merlin and S. R. Phillpot, *J. Appl. Phys.*, 2003, **93**, 793.

8 P. E. Hopkins, *ISRN Mech. Eng.*, 2013, **2013**, 682586.

9 D. G. Cahill, P. V. Braun, G. Chen, D. R. Clarke, S. Fan, K. E. Goodson, P. Keblinski, W. P. King, G. D. Mahan, A. Majumdar, H. J. Maris, S. R. Phillpot, E. Pop and L. Shi, *Appl. Phys. Rev.*, 2014, **1**, 011305.

10 S. Merabia and K. Termentzidis, *Phys. Rev. B*, 2014, **89**, 54309.

11 C. Monachon, L. Weber and C. Dames, *Annu. Rev. Mater. Res.*, 2016, **46**, 433.

12 J. Zhang, C. A. Polanco and A. W. Ghosh, *J. Heat Tran.*, 2018, **140**, 092405.

13 R. Rastgarkafshgarkolaei, Y. Zeng and J. Khodadadi, *J. Appl. Phys.*, 2016, **119**, 205107.

14 K. Aryana and M. B. Zanjani, *J. Appl. Phys.*, 2018, **123**, 185103.

15 Z. Wei, F. Yang, K. Bi, J. Yang and Y. Chen, *Carbon*, 2019, **144**, 109.

16 R. Ma, X. Wan, T. Zhang, N. Yang and T. Luo, *ACS Omega*, 2018, **3**, 12530.

17 M. D. Losego, M. E. Grady, N. R. Sottos, D. G. Cahill and P. V. Braun, *Nat. Mater.*, 2012, **11**, 502.

18 G. T. Hohensee, R. B. Wilson and D. G. Cahill, *Nat. Commun.*, 2015, **6**, 6578.

19 A. J. Schmidt, K. C. Collins, A. J. Minnich and G. Chen, *J. Appl. Phys.*, 2010, **107**, 104907.

20 C. B. Saltonstall, C. A. Polanco, J. C. Duda, A. W. Ghosh, P. M. Norris and P. E. Hopkins, *J. Appl. Phys.*, 2013, **113**, 13516.

21 J. C. Duda, C.-Y. P. Yang, B. M. Foley, R. Cheaito, D. L. Medlin, R. E. Jones and P. E. Hopkins, *Appl. Phys. Lett.*, 2013, **102**, 081902.

22 M. Jeong, J. P. Freedman, H. J. Liang, C.-M. Chow, V. M. Sokalski, J. A. Bain and J. A. Malen, *Phys. Rev. Appl.*, 2016, **5**, 014009.

23 E. Lee, T. Zhang, T. Yoo, Z. Guo and T. Luo, *ACS Appl. Mater. Interfaces*, 2016, **8**, 35505.

24 T. S. English, J. C. Duda, J. L. Smoyer, D. a. Jordan, P. M. Norris and L. V. Zhigilei, *Phys. Rev. B: Condens. Matter Mater. Phys.*, 2012, **85**, 035438.

25 Z. Tian, K. Esfarjani and G. Chen, *Phys. Rev. B: Condens. Matter Mater. Phys.*, 2012, **86**, 235304.

26 C. A. Polanco, R. Rastgarkafshgarkolaei, J. Zhang, N. Q. Le, P. M. Norris, P. E. Hopkins and A. W. Ghosh, *Phys. Rev. B*, 2015, **92**, 144302.

27 K. Saaskilahti, J. Oksanen, J. Tulkki and S. Volz, *Phys. Rev. B: Condens. Matter Mater. Phys.*, 2014, **90**, 134312.

28 Z. Liang and H.-L. Tsai, *J. Phys.: Condens. Matter*, 2011, **23**, 495303.

29 J. Smoyer, *PhD thesis*, University of Virginia, 2015.

30 C. A. Polanco and A. W. Ghosh, *J. Appl. Phys.*, 2014, **116**, 083503.

31 C. A. Polanco, R. Rastgarkafshgarkolaei, J. Zhang, N. Q. Le, P. M. Norris and A. W. Ghosh, *Phys. Rev. B*, 2017, **95**, 195303.

32 E. Lee, T. Yoo and T. Luo, ITherm 2017 Proceedings, 2017, p. 368.

33 H. K. Raut, V. A. Ganesh, A. S. Nair and S. Ramakrishna, *S. Energy Environ. Sci.*, 2011, **4**, 3779.

34 N. Q. Le, C. A. Polanco, R. Rastgarkafshgarkolaei, J. Zhang, A. W. Ghosh and P. M. Norris, *Phys. Rev. B*, 2017, **95**, 245417.

35 S. Datta, *Quantum Transport: Atom to Transistor*, Cambridge university press, 2005.

36 P. B. Clapham and M. C. Hutley, *Nature*, 1973, **244**, 281.

37 C. Bernhard, *Endeavour*, 1967, **26**, 79.

38 Y. Zhou, X. Zhang and M. Hu, *Nanoscale*, 2016, **8**, 1994.

39 C. Jeong, S. Datta and M. Lundstrom, *J. Appl. Phys.*, 2012, **111**, 93708.

40 A. Ghosh, *Nanoelectronics: A Molecular View*, World Scientific Publishing Company, 2016.

41 N. Mingo and L. Yang, *Phys. Rev. B*, 2003, **68**, 245406.

42 J.-S. Wang, J. Wang and J. T. Lü, *Eur. Phys. J. B*, 2008, **62**, 381.

43 C. A. Polanco, C. B. Saltonstall, P. M. Norris, P. E. Hopkins and A. W. Ghosh, *Nanoscale Microscale Thermophys. Eng.*, 2013, **17**, 263.

44 C. L. Wu, W. C. Hsu, H. M. Shieh and W. C. Liu, *Appl. Phys. Lett.*, 1994, **64**, 3027.

45 S. Keller, H. Li, M. Laurent, Y. Hu, N. Pfaff, J. Lu, D. F. Brown, N. A. Fichtenbaum, J. S. Speck, S. P. DenBaars *et al.*, *Semicond. Sci. Technol.*, 2014, **29**, 113001.

46 A. Grimshaw, M. A. Prodhan, A. Thomas, C. Stewart and R. Knepper, 2016 IEEE 12th International Conference on e-Science, 2016, p. 1.